Journal of The Electrochemical Society, **162** (10) H753-H758 (2015)
0013-4651/2015/162(10)/H753/6/$33.00 © The Electrochemical Society

A Drift-Diffusion Study on Charge Unbalancing Effects in Dye-Sensitized Solar Cells

Desirée Gentilini,[a,z] Alessio Gagliardi,[b] Alejandro A. Franco,[c,d,*] Frédéric Sauvage,[c,d] and Aldo di Carlo[a]

[a]*Universitá di Roma Tor Vergata, Department of Electronic Engineering, 00133 Rome, Italy*
[b]*Technische Universität München, Electrical Engineering and Information Technology, 80333 München, Germany*
[c]*Laboratoire de Réactivité et de Chimie des Solides (LRCS), UMR CNRS 7314, Université de Picardie Jules Verne, 80039 Amiens Cedex, France*
[d]*Réseau sur le Stockage Electrochimique de l'Energie (RS2E), FR CNRS 3459, France*

This work describes a modeling investigation of a working Dye-sensitized Solar Cells, including the contribution of ionic drift in the mass transport process of I_3^-/I^- redox couple. We found that the effective built-in electric field profile inside the cell is influenced by the density and distribution of the electronic traps located below the conduction band edge of the TiO_2. Although the value of electric field remains low compared to conventional p-n junction solar cells, our results support that the high concentration of ionic species composing the electrolyte prompts a drift current of ionic species, comparable to the related ionic diffusion current, when the device is exposed to light illumination under short-circuit conditions. The simulations carried out for different electrolyte compositions tend to demonstrate that ionic drift is a process which can never been suppressed and therefore should be considered in the description of the mass transport. These results participate in the better understanding of the working principle of the complex and multifaceted chemistry of dye-sensitized solar cells.

Manuscript submitted March 31, 2015; revised manuscript received June 30, 2015. Published July 14, 2015.

Dye-sensitized solar cell (DSC)[1] is a hybrid inorganic/organic photovoltaic technology which promised to rapidly meet low-cost energy production from sunlight and up-scalable processes for easy manufacturing. Nowadays, small active area cells developed in laboratories have reached up to 13.0%[2] power to conversion efficiency under standard illumination conditions (A.M 1.5G). Excellent stability reaching the threshold of 10% have been also reported testifying of the DSC viability for practical applications.[3,4] Pre-industrial modules are now meeting IEC61646 accelerating protocol.[5] This achievement has to be attributed to the large mutual effort to develop reliable and efficient DSC components.

However, many aspects of the device operating mechanisms remain under debate owing to the complexity of the underlying physical processes and the strong interplay between the different materials composing the cell. A complete understanding of all the different mechanisms involved in photoconversion is still lacking. Concerning the carriers transport processes in the cell, the diffusion model is widely accepted to describe the electron charge transport throughout the mesoporous layer of anatase TiO_2.[6] The general assumption made by the community is that the the overall charge neutrality (electronic + ionic) in a DSC is maintained through the high ionic strength in the electrolyte[7] which hinders the built-in of internal electric field, namely the electromigration of the electrons and the iodide species. This confers to the mass transport a pure diffusive character where the ions are moving freely solely under a gradient of concentration. Actually in the near field of electrochemical devices for energy conversion and storage (eg. fuel cells and Li-ion batteries), it has been demonstrated that the mass transport can be properly described using a multi-scale model approach.[8,9] These devices exhibits a similar mesoscopic structure of the electrode as in DSC, namely conductive or semi-conductive porous active materials filled by a liquid electrolyte. This similarity suggests that in DSC such electrode/electrolyte can be correctly modeled using a complete model, where all the driving forces for charges as diffusion and electro-migration are considered.

By contrast, in actual DSC modeling, the presence of a variable electrostatic potential is generally limited to the description of the electrode charge transfer,[10] whereas it has been pointed out that the macroscopic electric field becomes predominant at light intensities beyond 1 sun.[11,12] In the same line, ambipolar diffusion models has been formulated taking into account that both ions and electrons are diffusing at different rates.[13] This process in turn requires a weak electric field for keeping the charge neutrality. The pure diffusion model has been extended analytically[14] and numerically[15] to include trap states in TiO_2 and the dynamic of charge recombination. It is widely used for the formulation of the transmission line model[16] as well as for electron diffusion length studies.[17] In light of actual development, it appears clear that a complete description of the transport processes occurring in the cell requires to encompass at once the concentration gradient and the electric field as driving forces. In this work we have developed a multiphysics numerical model to account at once for the charge carriers transport, electric field, traps and generation/recombination processes which we are treated simultaneously. The scope of the present work is to provide new insights, from a modeling point of view and from general understanding, of mass transport description in Dye-sensitized Solar Cells.

Model

The simulation framework adopted to model the device is a Finite Element Drift Diffusion, implemented in the TiberCAD software.[18] It has been already used to investigate several aspects of standard DSCs, including new device architectures as integrated tandem DSC[19] and three-dimensional ring-shape DSC.[20] Experimental results are reproduced with high accuracy[21] providing reliable parameters for the equations resolution.

The model went through a development process over the years, starting from the first work[22] based on Ref. 23 and corresponding to the development of the main core of the model. A later work includes trap states in an effective way, in a Multi-trapping (MT) model.[21] In this work we present some recent evolution concerning the introduction of a real trap density of states, allowing to get rid of the effective density approximation as in the MT model. This latter implementation allows including in the simulation generic density of trap states located in the energy bandgap. The active layer of a DSC is constituted of crystalline TiO_2 nanoparticles sensitized by a dye monolayer whose functionality lies in the visible light capture and conversion to excitons. The nanoparticles form a continuous percolating porous structure of generally 10 μm thick in which the mesoporosity is completely filled by a liquid electrolyte. For our simulations, we are considering an effective material approximation. The active layer is described as a single homogeneous material phase having simultaneously the electrical and the optical properties of the TiO_2, dye and electrolyte. A schematic representation of a working cell is shown in Fig. 1. The most important assumption at the basis of the effective material approximation is that the electrostatic potential difference at the TiO_2/dye/electrolyte

*Electrochemical Society Active Member.
[z]E-mail: gentilini@ing.uniroma2.it

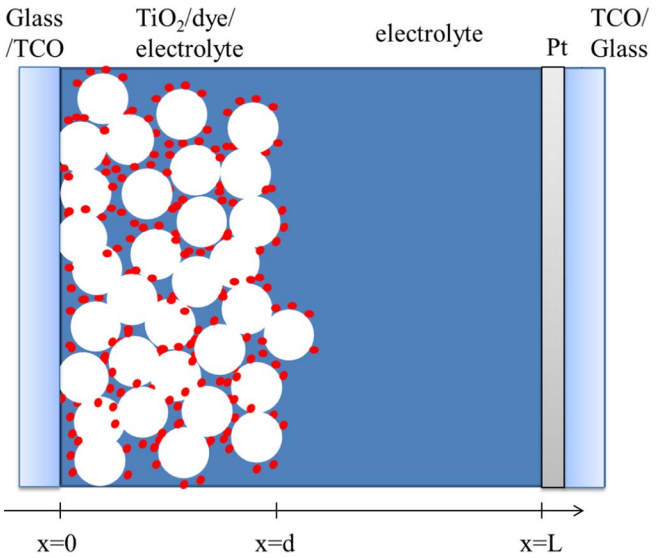

Figure 1. Scheme of the cell. The electron collector is at the TCO/TiO_2 interface, namely at $x = 0$. The counter-electrode is placed at Pt/TCO interface at $x = L$. The TiO_2/dye/electrolyte included between 0 and d is modeled as an effective medium, whereas the region between d and L is treated as bulk electrolyte.

interface is assumed to be spatially homogeneous along the active layer thickness. This potential difference is lumped in the definition of the band edges of the effective medium. This approach has been widely used for inorganic semiconductors, Organic Solar Cells[24] and Dye Solar Cells.[23] The presence of a porous interface in DSC with solid electrolyte has been simulated considering the real interface in our previous work.[25] We can claim that the effective model for a porous medium is a valid approximation when both materials involved are characterized by a high permittivity, which is the case of standard DSC. Therefore effects of microscopic electric fields in the cell such as electrochemical double layer formed at the interface between the TiO_2/dye and the electrolyte are neglected. In addition, all the processes which in a real DSC occurring at the interface are replaced by an effective bulk model to describe the recombination process and the dye regeneration. We are therefore considering effects of effective macroscopic electric field due to unbalancing of charge distribution in illuminated cells. The core of the model is a general constitutive equation (Eq. 1) for the flux density j_γ for each charge carrier:

$$j_\gamma = -D_\gamma \nabla n_\gamma + \mu_\gamma n_\gamma \nabla \varphi \qquad [1]$$

The index γ stands for the four charged species present in a DSC included in the calculation and are enlisted in Table I. Electrons (e^-), iodide (I^-), tri-iodide (I_3^-) participate to the current, while the positive counter-ion (C^+) is needed to ensure the electroneutrality of the entire cell. D_γ is the diffusion coefficient, n_γ the γ-charge carrier density, μ_γ the mobility and φ is the electrostatic potential. All the charges are assumed to satisfy the Einstein relationship associating diffusion coefficient and charge mobility:

$$D_\gamma = \frac{k\mathrm{T}}{q}\mu_\gamma. \qquad [2]$$

The driving force for charged particles, namely the electrons in the TiO_2 and ionic species in the electrolyte, is the gradient of their electrochemical potentials,[e] which includes both the chemical potential for particle accumulation and the electric field induced by local charge density. The resolution of Poisson equation allows to calculate the electric field and the distribution of the electrostatic potential across the whole cell depth.

The constitutive equations are therefore coupled to the Poisson equation and solved in terms of electrochemical potential ϕ_γ

$$\nabla \cdot j_\gamma = \nabla \cdot (\mu_\gamma n_\gamma \nabla \phi_\gamma) = \Lambda_\gamma (G - R) \qquad [3]$$

$$\nabla \cdot (\varepsilon \nabla \varphi) = -q[n_{C^+} + n_{D^+} - n_{I^-} - n_{I_3^-} - (n_e - \bar{n_e}) - n_t] \qquad [4]$$

where G and R are the generation and recombination rate respectively. Λ_γ is the stoichiometric coefficient which is linked to the chemical reaction of the different species to recombination and generation, and its value is reported in Table I for different species. In Eq. 4, q is the elementary charge and ε the dielectric constant which is assumed to be homogeneous in the effective material and it is calculated following the Maxwell-Garnet approximation for mixed mesoporous media.[22] n_{D^+} represents the steady state concentration of ionized dyes in the cell,[26] which is generally very low at standard light intensities, $\bar{n_e}$ is the equilibrium concentration of electrons in the TiO_2, equal to the intrinsic doping of the oxide, and n_t the trapped electron density.

An important role in DSC is played by trapped electron density in TiO_2. It has been demonstrated theoretically[27] and through comparison with experimental data[28,21] that electron trapping is not influencing the steady state electron transport, as long as trapped charges are not involved in the recombination process or supplying an additional pathway for transport via hopping mechanism. Therefore the effect of traps can be treated analytically in a pure diffusion model considering a distribution of localized states below the TiO_2 conduction band edge, where trapped electrons are in equilibrium with those in the conduction band and can be released by thermal activation. This analytical approach (Multi Trapping Model,[29] MTM) is valid as long as the electric field in the cell is negligible. In this paper we still assume that trapped states are not involved in transport. Concerning recombination, despite recombination via trapped state is possible,[30] we assume that recombination between via trapped electrons is negligible respect to recombination via conduction band electrons and its contribution can be accounted by correcting the recombination rate by non-ideality factor in Eq. 7.[31] The novelty consists in including into the model the key parameter of trapped states not in an effective way but inserting an exponential density of states below the conduction band edge of the TiO_2:

$$n_t = \int_{-\infty}^{E_c} f_{FD} N_t e^{-\frac{a(E-E_c)}{kT}} dE \qquad [5]$$

where N_t is the effective density of trapped states and a is describing the energy depth of the distribution under the conduction band edge (E_c), and f_{FD} is the Fermi-Dirac distribution function. As in MTM, we assume that the conduction band and the trapped electrons are in thermodynamic equilibrium,[29] meaning that the trapping-detrapping is faster than any other process. We will show that electron trapping can indeed influence the electrostatics of the device.

Photoelectron generation is accounted in the model with a Lambert-Beer approximation:

$$G(x) = \int_{\lambda_{min}}^{\lambda_{max}} \Phi(\lambda)\alpha(\lambda)e^{-\alpha(\lambda)x} d\lambda \qquad [6]$$

Table I. List of parameters used to simulate a working DSC.

Charged Species	Symbol γ	Recombination coefficient Λ_γ
electrons	e^-	1
iodide	I^-	−1.5
tri-iodide	I_3^-	0.5
cation	C^+	0

[e]The electrochemical potential ϕ_γ of a species γ with charge $z_\gamma q$ is defined as:

$$\phi_\gamma = \phi_\gamma^0 + k_B \mathrm{T} ln \frac{n_\gamma}{n_\gamma^0} + z_\gamma q \varphi$$

where φ is the inner electrostatic potential, n_γ is the concentration of the species and n_γ^0 is the concentration of some reference state for which the chemical potential takes its standard value ϕ_γ^0.

where $\Phi(\lambda)$ is the AM1.5 solar spectrum, and $\alpha(\lambda)$ is the dye absorption spectrum chemisorbed on the mesoporous medium, which can be extracted experimentally using a layer-by-layer spectroscopy measurement.[32] Light absorption is assumed to occur by the charge-transfer in the dye only. Absorption by direct interband excitation of TiO_2 or the absorption of I_3^- in the blue spectral range are not considered.

The predominant recombination path in the cell takes place at the TiO_2/electrolyte interface involving the reduction of I_3^- by conduction band electrons in TiO_2.[33] This recombination rate (R) is given by

$$R = k_e \left[n_e^{\beta} \frac{n_{I_3^-}}{n_{I^-}} - \bar{n}_e^{\beta} \sqrt{\frac{n_{I_3^-} \bar{n}_{I_3^-} n_{I^-}}{\bar{n}_{I^-}^3}} \right] \quad [7]$$

with k_e the recombination constant and $\bar{n}_\gamma$ the relative dark densities for each species. The parameter β can be identified as the non ideality factor described in several works, which could account for the recombination with surface states.[31]

Finally, for boundary conditions we use the following relations. No electrons from the TiO_2 can be collected by the counter-electrode (the cathode), i.e. following the notation in Fig. 1 $\nabla\phi_e|_{x=L} = 0$ and no ionic species can exchange charges with the anode collector, i.e. $\nabla\phi_{I^-}|_{x=0} = \nabla\phi_{I_3^-}|_{x=0} = 0$. The counter-ion does not contribute to the external current ($\nabla\phi_{C^+}|_{x=0,x=L} = 0$ both at the electrode and counter-electrode). No charge accumulation occurs at the contacts ($\nabla\varphi|_{x=0,x=L} = 0$).

The counter electrode is constituted by a thin layer of platinum nanoparticles deposited on the conductive glass. This layer acts as a catalyst to reduce the activation anergy required for I-I bond breaking to reduce tri-iodide to iodide. The kinetic aspect of this charge transfer reaction is following the Butler-Volmer equation. The boundary conditions for iodide and tri-iodide ions are:

$$J_{I^-} = \frac{3}{2} J_0 [e^{\frac{q\eta}{2kT}} - e^{-\frac{q\eta}{2kT}}] \quad [8]$$

$$J_{I_3^-} = -\frac{1}{2} J_0 [e^{\frac{q\eta}{2kT}} - e^{-\frac{q\eta}{2kT}}]. \quad [9]$$

In the Equations 8 and 9, the current is distributed according to the stoichiometry of the redox reaction. η is the overvoltage at the cathode and J_0 the exchange current.

The last boundary condition concerns the carriers at the TCO interfaces with electrolyte and TiO_2. An ideal contact shows very low resistance between TCO and TiO_2 film, and impedes the electron transfer to the electrolyte. Therefore we impose no ionic current flowing at the TCO/electrolyte interface and we consider a perfect ohmic contact for the electrons at the anode collector, imposing $\phi_e = q V_{ext}$. V_{ext} is the voltage between the contacts and q is the elementary charge.

Results and Discussion

Electrostatic influence of electron trapped states.— Using the multiscale model described in the previous section, in this part we show the effect of an increase of density of trapped electrons on the distribution of charges in the active layer and in the bulk electrolyte of a standard DSC. The calculation are performed at short-circuit at 1 sun illumination. The results are obtained adopting the parameterizations in Table II, which was carefully extracted from a detailed comparison of the model with the experimental data.[21]

Figure 2 shows the calculated charge density profiles inside a DSC at 1 sun illumination intensity for short circuit condition, considering three different situations. The *a* plot describes a cell where no electrons are trapped, whereas in *b* and *c* plots a stepwise increase in the density of traps ($N_t = 10^{20}$ cm^{-3}, $N_t = 10^{21}$cm^{-3}) is considered. The geometric interface between the effective medium and the bulk electrolyte presents some numerical oscillations, due to the abrupt change in porosity. In absence of traps, the electrons show a depletion profile toward the anode contact interface. We want to underline that this concentration gradient is responsible for the electron diffusion current, represented by the first term of Eq. 1. Even though, the ionic charge densities feature a relative flat evolution all along the cell, regardless the type of ionic species. The ionic species are therefore only slightly perturbed by the current generated by the photoelectrons.

Table II. List of parameters used to simulate a working DSC.

Parameter	Value	Units
μ_e	1	$[cm^2/Vs]$
k_e	1000	$[s^{-1}]$
D_{I^-}	10^{-5}	$[cm^2/s]$
$D_{I_3^-}$	10^{-5}	$[cm^2/s]$
$\bar{n}_{I^-}$	0.45	[Mol/l]
$\bar{n}_{I_3^-}$	0.05	[Mol/l]
N_t	10^{20}-10^{21}	$[cm^{-3}]$
a	0.3	[−−]
$porosity$	0.5	[−−]
J_0	0.1	$[A/cm^2]$

The implementation of this calculation with the occurrence of a modest density of traps ($N_t = 10^{20}$ cm^{-3} Fig. 2b, comparable with other works[34]), seems to not significatively alter the distribution of charges inside the cell. Nevertheless, the presence of electrons trapped

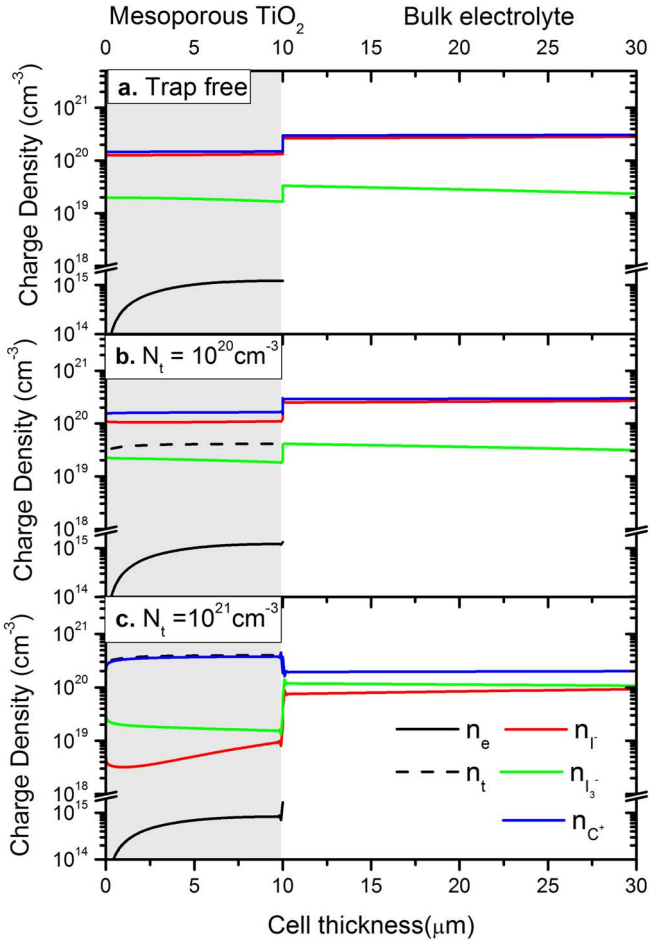

Figure 2. Calculated density profiles are reported for each charge species in a DSC with 10 μm of TiO_2 and 20μm of bulk electrolyte. Conduction band electrons (black) trapped electrons (dashed black), iodide (red) tri-iodide (green) and the positive cation (blue) are plotted. The profiles are shown in absence of traps (a) and for a trap density $N_t = 10^{20}$ cm^{-3} (b) and $N_t = 10^{21}$ cm^{-3} (c). Calculations are performed at short-circuit condition at 1 sun illumination.

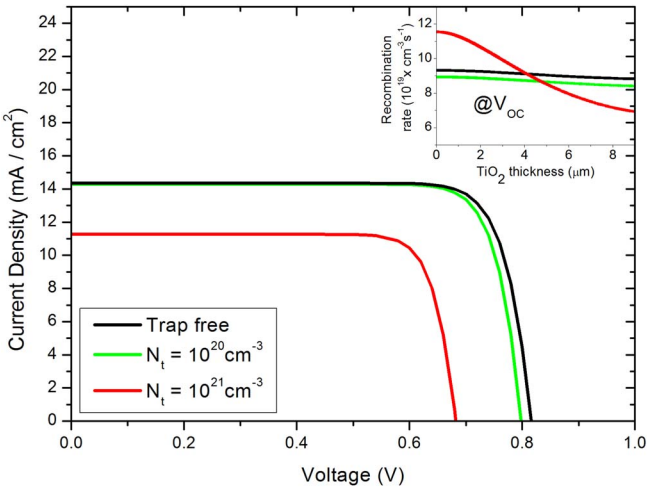

Figure 3. Calculated J-V characteristics in absence of traps (black line), with medium (green) and high (red) concentration of traps. The inset shows the recombination rate profile calculated at open-circuit voltage for the three cases.

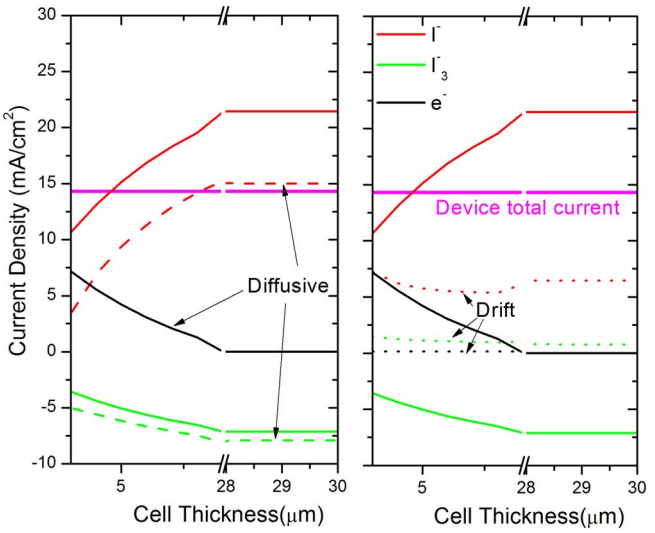

Figure 4. Current density profiles for electrons (black) iodide (red) and tri-iodide (green) are reported in both plots (solid lines). Left plot reports the diffusive (dash) contributions to the total current and the right plot reports the drift (dot) ones. Electronic diffusive current coincides with the total one. The total current of the cell is represented by the pink line.

in the exponential tail forces the positive ion charges to redistribute along the cell. At short circuit the free electron density is bended toward the collector. Since trapped and conduction band electrons are assumed to be in equilibrium, the bending of the two profiles follows the same feature. In this case, the negatively charged electron density (free and trapped) is much larger respect to the case of no traps. This induces the double effect of pushing I_3^- in the bulk electrolyte and pulling of the positive cation density toward the mesoporous medium. Here the cation follows the electronic depletion as well, in order to assure charge neutrality. Since no cationic current at the anode collector is allowed to flow, (electrochemical potential of C^+ is set to be zero at x = 0) the density bending of the cation corresponds to a modification of the electrostatic potential. As a consequence, a weak electric field appears at the collector interface ($\sim$1-10 V/cm).

Examining the J-V characteristics in Fig. 3, the electric field at the collector does not alter the J_{sc}. However the cell with $N_t = 10^{20}$ cm^{-3} presents a slight but noticeable reduction of the V_{oc} value by 20 mV. In order to explain the motivation of this reduction, we calculated the recombination rate profile along the mesoporous medium (inset in Fig. 3), finding that the cell with higher open-circuit voltage presents surprisingly higher recombination. Actually the presence of traps pushes the electron Fermi level inside the gap away from the conduction band edge, lowering the free electron density respect to the case of a trap-free TiO_2. This has the two-fold effect of reducing the recombination rate, which is proportional to the free electron density in Eq. 7, and decreasing the final V_{oc} value. Finally, in presence of modest quantity of trapped states the cell J-V characteristics is slightly perturbed by the redistribution of ionic species, revealing that the screening strength of the electrolyte is preserved.

The distribution of charges in the electrolyte is more drastically influenced when the density of trapped electrons become higher than the concentration of ions in the electrolyte (Fig. 2c). This high electron density can experimentally take place when there is a lack of percolation among the TiO_2 nanoparticles (eg. electrode too porous or bad sintered) or when the cell is exposed to light intensity higher than 1 sun. In this particular case, the cations cannot efficiently screen the excess of negative charges in the TiO_2. It results a weak electric field appearing not only within the mesoporous medium, but in the whole cell profile ($\sim$0.1 V/cm). In fact, the high amount of trapped electrons in TiO_2 entails an important depletion in the other negative species (I^- and I_3^-) toward the bulk electrolyte, enforced by an accumulation of positive cation in the mesoporous region. This spatial charge redistribution in the device has a detrimental effect on its J-V characteristics, as shown with the red curve in Fig. 3. In this case the free electrons density in the conduction band state is severely reduced, and this, as previously remarked, should decrease the recombination. Actually the redistribution of ionic charges due to the electric field, makes the I_3^-/I^- ratio more relevant in the recombination rate Eq. 7, resulting in an overall augmented and detrimental recombination (inset Fig. 3).

In order to limit the formation of this harmful internal electric field, a high concentration of supporting salt is required to enhance the ionic strength of the electrolyte. Even though, we would like to stress that the appearance of a macroscopic electric field results even from a fine balancing of electron density (both free and trapped) and the concentration of ions in the electrolyte.

Drift current calculation.— The calculated amplitude of the macroscopic electric field and the electron density inside a DSC cell are rather low compared to drift-driven PV device such as p-n silicon solar cell. Indeed, thin film amorphus silicon can present an electric field up to $\sim 10^4$ - 10^5 V/cm.[35] The electric field is responsible for the migration of carriers along the cell, in particular the drift current is the product of the electric field and the charge density and it is represented by the second term in Eq. 1.

We calculate the current density profiles for each charge carrier and reported the results in Fig. 4. The total current of a DSC device results from the sum of drift current and diffusion current for each charged species. In order to fulfill the charge conservation, the total current must be constant throughout the device.

The fluxes of oxidized an reduced species in the electrolyte are flowing in opposite directions. I_3^- is flowing from the photo-anode to the counter-electrode (giving a negative current) and I^- moves from the counter-electrode to the photo-anode, thus providing a positive current by convention. We can extract then the contribution to the total current of the diffusive and drift components. For what concerns electrons, only conduction band electrons participate to transport, therefore the electronic drift current in DSC is negligible. This has been previously demonstrated theoretically[6] and through a comparison with the experimental data.[21] On the other hand, ions in DSC present a far larger density respect to free electrons (Fig. 2), therefore even though the electric field is weak, it generates a non negligible ionic migration current.

For the I^- the drift is representing the 30% of the total I^- current, whereas it is the 10% for I_3^- owing to the net charge density difference of the two anions (Fig. 2). The drift component of the current of both species is positive accordingly to the electric field. The behavior

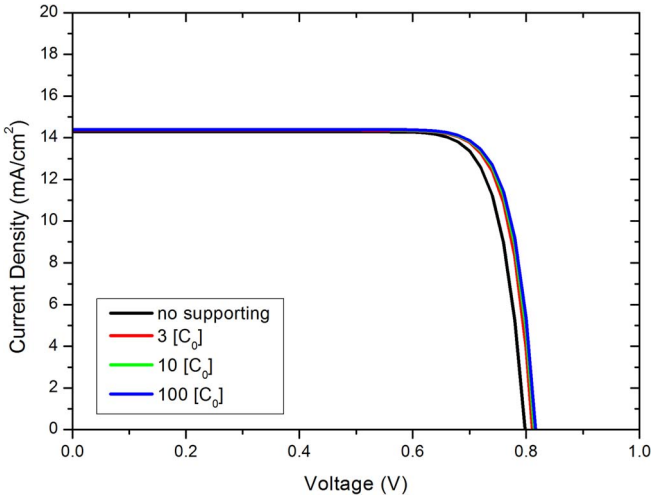

Figure 5. Current voltage characteristics calculated with an enhanced molarity of initial iodide and tri-iodide concentration.

discussed above is now calculated in a more realistic device in presence of supporting electrolyte. In order to quantify the influence of these additives on the electric field, we increased the concentration of the existent ionic species (already implemented in the code), considering the effect on the Poisson equation only. The initial molarity of I^-, I_3^- and C^+, noted $[C_0]$, has been increased of 1 and 2 orders of magnitude.

The J-V characteristic profiles (shown in Fig. 5) are unaltered by the presence of such a high density of I^-, I_3^- and C^+ meaning that all the ionic charges in excess does not contribute to the photo-current and are actually inert for the generation/recombination process. Their role consists mechanistic to screen the macroscopic electric field, which is exactly the role played by an inert supporting salt in electrolyte. This expedient allows us to avoid implementing some more equation in the code to include other inert additives, which is computationally very expensive.

In Fig. 6 the drift ionic currents are finally reported as a function of the inverse of the electric field for I^- and I_3^- with increasing concentration of ionic species. In order to avoid to include additional effects induced by high electric field at the collector, we calculated

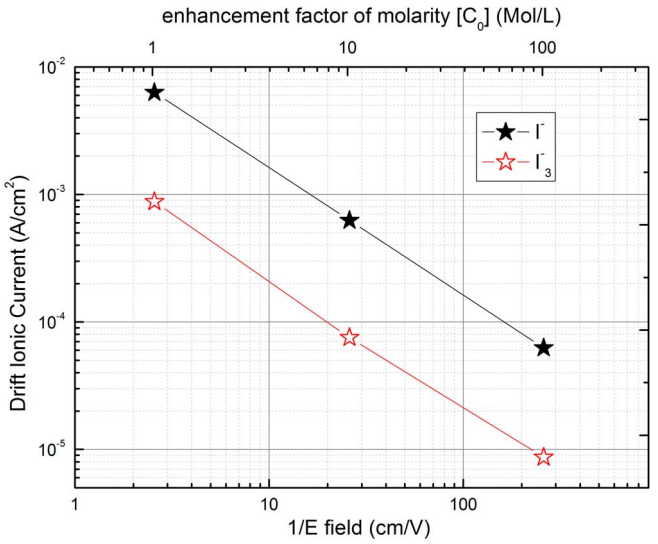

Figure 6. Drift current of I^- (black) and I_3^- (red) are plotted in function of the inverse of mean electric field for three different concentrations of supporting electrolyte.

the mean value of the electric field in the bulk electrolyte side only. As expected, the drift component of the current decreases with a high density of ions in solution. Experimentally the concentration of supporting additives lies in a range of 0.1-1 Mol/L,[36] therefore we can conclude from this work that the ionic drift component of the current cannot be completely suppressed in a working DSC under standard illumination.

Conclusions

In this work we have made use of a drift-diffusion model to provide new insights about the current description of the mass transport in a DSC under operation. We consider out from the model the evolution of the electrostatic field in the cell for different density of trapped electron in TiO_2. The main outcome stems from the demonstration of a non-negligible iodide drift current taking place in the mesoporous medium filled by electrolyte. On the other hand, when the supporting electrolyte is included in the simulation, the drift ionic current can be suppressed, but only for very large concentration of additives. This findings shed light not only on the role of additives as supporting electrolyte but also on the importance of charge unbalancing in the photoelectrochemical DSC device.

Acknowledgment

The author thank the Center of Hybrid and Organic Solar Energy (CHOSE) for funding this work. FS is indebted to the FEDER and region Picardie for funding the research program.

References

1. B. O'Regan and M. Gratzel, *Nature*, **353**, 737 (1991).
2. S. Mathew, A. Yella, P. Gao, R. Humphry-Baker, B. F. E. Curchod, N. Ashari-Astani, I. Tavernelli, U. Rothlisberger, M. K. Nazeeruddin, and M. Grtzel, *Nature Chemistry*, **6**, 242 (2014).
3. F. Sauvage, S. Chhor, A. Marchioro, J.-E. Moser, and M. Graetzel, *Journal of the American Chemical Society*, **133**, 13103 (2011).
4. Q. Yu, D. Zhou, Y. Shi, X. Si, Y. Wang, and P. Wang, *Energy Environ. Sci.*, **3**, 1722 (2010).
5. A. Fakharuddin, R. Jose, T. M. Brown, F. Fabregat-Santiago, and J. Bisquert, *Energy Environ. Sci.*, **7**, 3952 (2014).
6. S. Soedergren, A. Hagfeldt, J. Olsson, and S.-E. Lindquist, *The Journal of Physical Chemistry*, **98**, 5552 (1994).
7. J. van de Lagemaat and A. J. Frank, *The Journal of Physical Chemistry B*, **105**, 11194 (2001).
8. M. A. Quiroga, K.-H. Xue, T.-K. Nguyen, M. Tulodziecki, H. Huang, and A. A. Franco, *J. Electrochem. Soc.*, **161**, E3302 (2014).
9. A. A. Franco, P. Schott, C. Jallut, and B. Maschke, *Fuel Cells*, **7**, 99 (2007).
10. A. Hauch and A. Georg, *Electrochimica Acta*, **46**, 3457 (2001).
11. K. Zhu, E. A. Schiff, N.-G. Park, J. van de Lagemaat, and A. J. Frank, *Applied Physics Letters*, **80**, 685 (2002).
12. G. Franco, J. Gehring, L. M. Peter, E. A. Ponomarev, and I. Uhlendorf, *The Journal of Physical Chemistry B*, **103**, 692 (1999).
13. D. Nister, K. Keis, S.-E. Lindquist, and A. Hagfeldt, *Solar Energy Materials and Solar Cells*, **73**, 411 (2002).
14. P. R. F. Barnes, A. Y. Anderson, S. E. Koops, J. R. Durrant, and B. C. O'Regan, *Journal of Physical Chemistry C*, **113**, 1126 (2009).
15. P. R. F. Barnes, A. Y. Anderson, J. R. Durrant, and B. C. O'Regan, *Phys. Chem. Chem. Phys.*, **13**, 5798 (2011).
16. F. Fabregat-Santiago, J. Bisquert, G. Garcia-Belmonte, G. Boschloo, and A. Hagfeldt, *Solar Energy Materials and Solar Cells*, **87**, 117 (2005).
17. J. Halme, G. Boschloo, A. Hagfeldt, and P. Lund, *The Journal of Physical Chemistry C*, **112**, 5623 (2008).
18. M. Auf der Maur, G. Penazzi, G. Romano, F. Sacconi, A. Pecchia, and A. Di Carlo, *IEEE Transactions on electron devices*, **58**, 1425 (2011).
19. R. Tagliaferro, D. Gentilini, S. Mastroianni, A. Zampetti, A. Gagliardi, T. M. Brown, A. Reale, and A. Di Carlo, *RSC Adv.*, **3**, 20273 (2013).
20. A. Gagliardi, M. Auf der Maur, D. Gentilini, and A. Di Carlo, *Journal of Computational Electronics*, **10**, 424 (2011).
21. D. Gentilini, A. Gagliardi, M. Auf der Maur, L. Vesce, D. D'Ercole, T. M. Brown, A. Reale, and A. Di Carlo, *The Journal of Physical Chemistry C*, **116**, 1151 (2012).
22. A. Gagliardi, M. Auf der Maur, D. Gentilini, and A. Di Carlo, *Journal of Computational Electronics*, **8**, 398 (2009).
23. J. Ferber, R. Stangl, and J. Luther, *Solar Energy Materials and Solar Cells*, **53**, 29 (1998).
24. A. Fallahpour, A. Gagliardi, D. Gentilini, A. Zampetti, F. Santoni, M. Auf der Maur, and A. Di Carlo, *Journal of Computational Electronics*, **13**, 933 (2014).

25. A. Gagliardi, M. Auf der Maur, D. Gentilini, F. di Fonzo, A. Abrusci, H. J. Snaith, G. Divitini, C. Ducati, and A. Di Carlo, *Nanoscale*, **7**, 1136 (2015).
26. A. Gagliardi, S. Mastroianni, D. Gentilini, F. Giordano, A. Reale, T. Brown, and A. D. Carlo, *IEEE Journal of Selected Topics in Quantum Electronics*, **16**, 1611 (2010).
27. J. A. Anta, F. Casanueva, and G. Oskam, *The Journal of Physical Chemistry B*, **110**, 5372 (2006).
28. Q. Wang, S. Ito, M. Grtzel, F. Fabregat-Santiago, I. Mora-Ser, J. Bisquert, T. Bessho, and H. Imai, *The Journal of Physical Chemistry B*, **110**, 25210 (2006).
29. J. Bisquert and V. S. Vikhrenko, *The Journal of Physical Chemistry B*, **108**, 2313 (2004).
30. M. Filipic, M. Berginc, F. Smole, and M. Topic, *Current Applied Physics*, **12**, 238 (2012).
31. J. Halme, P. Vahermaa, K. Miettunen, and P. Lund, *Advanced Materials*, **22**, E210 (2010).
32. Y. Tachibana, K. Hara, K. Sayama, and H. Arakawa, *Chemistry of Materials*, **14**, 2527 (2002).
33. P. R. F. Barnes, L. Liu, X. Li, A. Y. Anderson, H. Kisserwan, T. H. Ghaddar, J. R. Durrant, and B. C. ORegan, *Nano Letters*, **9**, 3532 (2009).
34. F. Cappelluti, S. Ma, D. Pugliese, A. Sacco, A. Lamberti, G. Ghione, and E. Tresso, *Phys. Chem. Chem. Phys.*, **15**, 14634 (2013).
35. M. Stuckelberger, A. Shah, J. Krc, M. Despeisse, F. Meillaud, and C. Ballif, *Photovoltaic Specialists Conference (PVSC), 2010 35th IEEE*, 001569 (2010).
36. S. Mastroianni, A. Lembo, T. M. Brown, A. Reale, and A. Di Carlo, *ChemPhysChem*, **13**, 2806 (2012).